



MPG-NET: A low-cost, multi-purpose GNSS co-location station network for environmental monitoring

Matthias Aichinger-Rosenberger^{a,c,*}, Alexander Wolf^a, Cornelius Senn^b, Roland Hohensinn^{a,d}, Marcus Franz Glaner^e, Gregor Moeller^a, Benedikt Soja^a, Markus Rothacher^a

^a Institute of Geodesy and Photogrammetry, Department of Civil, Environmental and Geomatic Engineering, ETH Zurich, Robert-Gnehm-Weg 15, Zurich, 8093, Switzerland

^b Department of Civil, Environmental and Geomatic Engineering, ETH Zurich, Laura-Hezner-Weg 7, Zurich, 8093, Switzerland

^c Constellation Observing System for Meteorology Ionosphere and Climate (COSMIC) Program, University Corporation for Atmospheric Research (UCAR), 3300 Mitchell Lane, Boulder, CO, 80301, United States of America

^d International Space Science Institute, Hallerstrasse 6, Bern, 3012, Switzerland

^e Research Unit Higher Geodesy, Department of Geodesy and Geoinformation, Technical University of Vienna, Wiedner Hauptstraße 8, Vienna, 1040, Austria

ARTICLE INFO

Dataset link: <https://gmc.ethz.ch>

Keywords:

Low-cost GNSS
Remote sensing
Environmental monitoring
GNSS-R
Water vapor retrieval
Soil moisture retrieval

ABSTRACT

Global Navigation Satellite Systems (GNSS) are very versatile sensors, which can be used for a variety of commercial and scientific applications. This holds especially true for different fields of remote sensing, such as atmospheric sounding or soil moisture monitoring. With the advent of low-cost dual-frequency GNSS equipment, certain applications are no longer restricted to the use of geodetic-grade instrumentation and can fully take leverage of the measurements in a second frequency band. In view of these emerging benefits, this study introduces the development and deployment of a multi-purpose GNSS station network in the Swiss Alps, called MPG-NET. We discuss the technical details of the station setup, in terms of GNSS hardware and technical design, as well as the quality of derived GNSS remote sensing products. In particular, our analyses focus on the quality of derived time series of zenith total delays (ZTD) and volumetric soil moisture content. Products are validated against benchmark data obtained from numerical weather models and in-situ sensors. For a prototype station, the results show a good agreement with the baseline, with errors of few millimeters for ZTD, and a remarkably high correlation for soil moisture content. Beside the documented value of low-cost GNSS for displacement monitoring (such as landslides or strong earthquakes), these findings are another step towards the establishment of a dense high-precision, multi-purpose GNSS network that comes at a very affordable price.

1. Introduction

Over the last decades, Global Navigation Satellite System (GNSS) technology has made impressive progress [1], resulting in a large number of scientific and industrial applications in various areas. Originally developed for positioning and navigation applications, GNSS are nowadays extensively used in a variety of research fields, especially in geosciences [2]. Although the measurement principle of GNSS is rather simple, a number of influences affecting the travel time of the signals have to be considered. This leaves potential users interested in positioning or navigation purposes with several nuisance signals, which need to be eliminated or determined alongside the user position. Some of these nuisance signals are of interest for GNSS remote sensing, with applications ranging from atmospheric sounding to the determination

of soil moisture or snow height in the vicinity of a GNSS station (e.g., [3,4]). This makes GNSS receivers/antennas a versatile sensor for environmental monitoring in a number of different research fields such as seismology, meteorology or hydrology (e.g., [5–7]).

Along with this broadening of GNSS applications in geosciences, capabilities of the specific hardware and software solutions have also been extended. State-of-the-art GNSS processing software has been developed [8,9], also for real-time applications such as Precise Point Positioning (PPP) [10–13]. Various software packages have become freely available [14,15], especially in the field of GNSS remote sensing [16]. Furthermore, there is a rapidly growing market for low-cost GNSS equipment, which is used extensively for positioning and navigation purposes. Applications range from autonomous driving, aviation

* Corresponding author at: Institute of Geodesy and Photogrammetry, Department of Civil, Environmental and Geomatic Engineering, ETH Zurich, Robert-Gnehm-Weg 15, Zurich, 8093, Switzerland.

E-mail address: maichinger@ethz.ch (M. Aichinger-Rosenberger).

<https://doi.org/10.1016/j.measurement.2023.112981>

Received 30 January 2023; Received in revised form 19 April 2023; Accepted 1 May 2023

Available online 6 May 2023

0263-2241/© 2023 The Author(s). Published by Elsevier Ltd. This is an open access article under the CC BY license (<http://creativecommons.org/licenses/by/4.0/>).

and smartphone positioning, to various use-cases in environmental monitoring (e.g., [17–21]). The rising demand of applications is accompanied by significant enhancements in sensor capabilities, in terms of GNSS receiver hardware as well as signal processing. Recent studies showed that GNSS measurements, collected using low-cost or medium-grade antennas, can reach accuracy levels comparable to those obtained with high-grade equipment (e.g., [22,23]). Low-cost single-frequency GNSS, used in relative positioning mode such as Real Time Kinematic (RTK), provides precision sufficient for many navigation applications, as well as for geodetic and geophysical monitoring purposes (e.g., [24–27]).

Over the last years, even low-cost dual-frequency (DF) receivers have become available. This DF upgrade enables the use of the ionosphere-free linear combination (IF-LC), which allows to mitigate most of the effects of the ionosphere on GNSS observations. The DF GNSS chipset ZED-F9P of the Swiss company u-blox is currently one of the most prominent products available. In recent studies, the performance of the DF low-cost devices, such as the ZED-F9P, has been studied for a variety of applications in geodetic and environmental science. For both, kinematic and static positioning with RTK and PPP modes, authors concluded that centimeter to millimeter level precision can be obtained using such instrumentation, also in combination with most recent low-cost GNSS antennas (e.g., [23,28,29]). Latter studies also pointed out that the performance of low-cost GNSS equipment approaches the performance of geodetic-grade equipment, especially when low-cost helical-type antennas are used. Recent studies also showed that dual-frequency low-cost GNSS modules can also successfully used for ionospheric monitoring [30], and even show very good results for the monitoring of ionospheric scintillations, when being compared to state-of-the-art geodetic-grade equipment [31].

DF receivers are especially instrumental for high-precision GNSS applications, such as PPP-enabled tropospheric delay estimation. This technique allows for an accurate sensing of atmospheric water vapor, and is typically referred to as GNSS meteorology (e.g., [6,32–34]). The performance of low-cost GNSS setups for troposphere monitoring was recently studied by a number of authors. Barindelli et al. [35] compared the performance of geodetic and low-cost GNSS receivers for the detection of temporal variations of water vapor associated with heavy rain in Northern Italy. They concluded that low-cost single-frequency receivers could be a promising solution for GNSS network densification, although some technological limitations still exist. One of the first studies on the usability of the ZED-F9P for tropospheric monitoring was carried out by Krietemeyer et al. [36], who analyzed ZTD estimates with a variety of antenna setups of different quality. They were able to show that the receiver module is capable of meeting accuracy requirements for usage in Numerical Weather Prediction (NWP) and concluded that a main limiting factor is the quality of the receiving antenna. For static GNSS experiments they could show that an accuracy of a few millimeters can be achieved in comparisons to geodetic-grade equipment. Stepniak and Paziewski [37] confirmed these findings by comparing solutions from the ZED-F9P using different antenna types to tropospheric delays from ray-tracing. In a recent study, Marut et al. [38] showed the usability of the ZED-F9P for retrieval of ZTD and integrated water vapor (IWV) in a very dense network, covering the city of Wrocław, Poland. Validation of their results using estimates from geodetic-grade GNSS receivers and a co-located water vapor radiometer showed satisfactory performance of the proposed station setup.

Soil moisture can be derived from ground-based GNSS by means of GNSS Interferometric Reflectometry (GNSS-IR), which is considered to be one of the most important methods in the class of GNSS reflectometry (GNSS-R) tools. The technique of GNSS-IR, which was introduced more than a decade ago [39], uses signal multipath and corresponding signal-to-noise ratio (SNR) to infer information on different environmental parameters in the vicinity of a GNSS station. The technique has been used to estimate soil-moisture-related parameters [40] as well as snow properties such as snow height ([41,42]) and snow water

equivalent [43]. For the retrieval of soil moisture from GNSS, one can take leverage of the fact that the phase of the SNR signal is linearly related to changes of the surface soil moisture (to approximately a soil depth of 5 cm) [44]. By this ground-based retrieval strategy, soil moisture variations in the vicinity of approximately 1000 m² around a GNSS station can be sensed. Using a multi-year GNSS data set, Vey et al. [45] were able to show that the GNSS-derived estimates correlate very well with soil moisture observations obtained from time-domain in-situ sensors. Their estimates achieved an accuracy of about 5% compared to the in-situ measurements. Chew et al. [46] derived a method to correct GNSS-derived soil moisture by vegetation effects in the vicinity of a station, and could thus further enhance the accuracy of the soil moisture estimation. However, only a small number of studies have yet used low-cost equipment for investigations on products from GNSS-IR. Fagundes et al. [47] developed a low-cost GNSS single-frequency sensor and software package for sea level altimetry studies. When compared to tide gauge data, they reported errors of few centimeters only. Similar sensors for reflector height estimation were developed by Li et al. [48] and Karegar et al. [49] by utilizing the u-blox M8N chip. Liu et al. [50] showed GNSS-IR altimetry results for a Huawei P30 smartphone in comparison to the results of a u-blox F9P with a low-cost antenna on the L1 frequency. They reported better results for the smartphone, which was attributed to a better multipath susceptibility of the linearly polarized smartphone antenna. However, none of the previous studies on low-cost GNSS-IR utilized dual-frequency data (especially L2 observations) for soil moisture retrieval. In addition to ground-based stations, kinematic airborne platforms have also been used for GNSS-IR. Ichikawa et al. [51] used low-cost GNSS equipment mounted on an unmanned aerial vehicle (UAV) platform for GNSS-R altimetry. They were able to achieve an accuracy in the order of one centimeter for water level estimates. Imam et al. [52] investigated the performance of UAV-based GNSS-R sensors for detecting surface water changes for a potential application in supporting flood monitoring operations. Their results for the area surrounding the Avigliana lakes in Northern Italy showed the possibility of detecting small water surfaces with few tens of meters resolution.

Based on the introduced studies and experience gained in former projects, we investigate the performance of a specific GNSS station setup, which was assembled especially for low-cost GNSS remote sensing. Besides the monitoring that is routinely done with such equipment (e.g., monitoring of slope movements or landslides [21]), there is a high potential for low-cost DF GNSS usage in remote sensing of the atmosphere and the hydrosphere. In the course of the pilot project MPG-NET (Multi-Purpose GNSS Network), initiated in cooperation with the Federal Office of Meteorology and Climatology of Switzerland (MeteoSwiss), a number of meteorological observation sites all over Switzerland are collocated with GNSS equipment. This study introduces the detailed GNSS payload deployed at the SwissMetNet (SMN) sites in the framework of the project, as well as initial results for troposphere and soil moisture products from a prototype station established at the SMN site Zurich-Affoltern (REH). The paper is organized as follows:

- Section 2 describes the methodology and theoretical foundations of GNSS-based troposphere and soil moisture monitoring. Furthermore, it introduces additional data sets used for validation of the GNSS products.
- Section 3 introduces the station setup, system design as well as test results for different sensor setups, on which the final solution is based.
- Section 4 presents initial results from the prototype site for troposphere and soil moisture products.
- Section 5 provides a detailed discussion of the results shown in Section 4.
- Section 6 summarizes the major findings and gives an outlook to the variety of planned future activities in the framework of MPG-NET.

2. Methodology and applications

This section describes the applications and products of MPG-NET. In the following, we detail two scientific research fields and approaches for which the introduced station setup can deliver valuable results. Furthermore, complementing infrastructure used in this study is introduced, including existing GNSS networks in Switzerland.

2.1. GNSS troposphere products

When traveling through the Earth's atmosphere, electromagnetic waves such as GNSS signals are delayed. This fact enables the monitoring of tropospheric parameters (in particular water vapor) using GNSS observations. The signal delay is directly proportional to the refractive index n or refractivity N of the atmosphere. The relationship between n and N is given by

$$N = (n - 1) \times 10^6. \quad (1)$$

N is composed of a hydrostatic (N_{hydr}) and wet part (N_w). A common formulation for it reads [53]:

$$N = N_{hydr} + N_w = k_1 \frac{R}{M_d} \rho + k_2 \frac{e}{T} Z_w^{-1} + k_3 \frac{e}{T^2} Z_w^{-1} \quad (2)$$

with:

$$k_2' = k_2 - k_1 \frac{M_w}{M_d} \quad (3)$$

and:

$$N_{hydr} = k_1 \frac{R}{M_d} \rho \quad (4)$$

$$N_w = k_2' \frac{e}{T} Z_w^{-1} + k_3 \frac{e}{T^2} Z_w^{-1} \quad (5)$$

where k_1, k_2, k_2', k_3 are empirical constants, R is the universal gas constant, ρ is dry air density, M_d and M_w are the molar mass of dry air and water vapor, Z_w is the compressibility factor for water vapor, T is temperature, and e is water vapor pressure.

For a GNSS signal, observed at an elevation el and azimuth direction a , the total tropospheric delay is referred to as the Slant Total Delay (STD)

$$STD(a, el) = ZHD \cdot m_{f_h}(el) + ZWD \cdot m_{f_w}(el) + m_{f_g}(el) \cdot [G_N \cdot \cos(a) + G_E \cdot \sin(a)] \quad (6)$$

where ZHD (Zenith Hydrostatic Delay) represents the hydrostatic part and ZWD the wet part of the signal delay in the zenith direction. In addition, horizontal gradients G_N (north–south direction) and G_E (east–west direction), accounting for the asymmetry of the atmospheric layers passed by the signal, can be estimated in the GNSS processing. In order to map the delays and gradients estimated for the zenith direction to the correct elevation, mapping functions for both parts of the delay ($m_{f_h}(el), m_{f_w}(el)$) and the gradients ($m_{f_g}(el)$) are used.

The total delay in the zenith direction, i.e. ZTD, is the sum of the hydrostatic and wet part

$$ZTD = ZHD + ZWD. \quad (7)$$

ZHD accounts for the major part of the total delay and is largely determined by the atmospheric pressure. It can be modeled with sufficient accuracy from surface pressure observations using, e.g., the formula of Saastamoinen [54]:

$$ZHD = \frac{0.0022767 \cdot p_s}{1 - 0.00266 \cdot \cos(2\theta) - 0.00028 \cdot H} \quad (8)$$

where p_s is the surface pressure, θ the station latitude, and H is the station height above the geoid.

ZWD is directly related to the water vapor content in the air column above the GNSS antenna and therefore denotes the most interesting parameter for meteorological proposes. It also shows the same high

Table 1

Overview of solution types for ZTD products shown in the comparisons of this section. Indicated are utilized orbit/clock products, software package and processing strategy.

| Solution type | Products | Software | Processing strategy |
|---------------------|-----------------------|-------------|---------------------|
| Post-processed (PP) | CODE final | Bernese 5.2 | PPP, static, float |
| Real-time (RT) | CNES real-time stream | raPPPid | PPP, static, float |
| COSMO-1 | | Python3 | Ray-tracing |

temporal and spatial variability as water vapor, which makes precise modeling from meteorological surface observations practically impossible. For this reason, ZWD is routinely estimated as an unknown in GNSS processing. A detailed description of the estimation process is provided in the following section.

2.1.1. GNSS data processing

The processing of GNSS raw data is carried out in static PPP [10,11] mode using multi-GNSS (Global Positioning System (GPS), Globalnaya Navigatsionnaya Sputnikovaya Sistema (GLONASS) and Galileo) observations at a sampling rate of 30 seconds. PPP processing is based on the IF-LC and the phase ambiguities are estimated as real numbers (float solution). Two different GNSS-based ZTD solutions using different software packages are produced. Furthermore, an independent reference solution, using output from an NWP model, is computed for validation proposes (see Section 2.1.2 for details). An overview of all solution types can be found in Table 1. A post-processing (PP) ZTD solution is produced using the Bernese GNSS software 5.2 [9], utilizing final orbit and clock products from the Center for Orbit Determination in Europe (CODE). The Global Mapping Function (GMF, [55]) is used as the tropospheric mapping function, ZHD is calculated using the Saastamoinen model (Eq. (8)) and residual ZWD is estimated hourly using least-squares based estimation. For future products, we plan to utilize the new Vienna Mapping Functions 3 (VMF3 [56]) together with pressure observations collected directly on-site to calculate ZHD. Station coordinates are estimated once per day in a similar way.

Furthermore, we utilize the open-source PPP software package raPPPid,^{1,2} [57] developed at Technical University Vienna as a part of the Vienna VLBI and Satellite Software (VieVS, [58]). Among other features, the software is capable of quasi-real-time PPP processing. We make use of this capability to produce a quasi-real-time (RT) ZTD solution, using the GNSS orbit and clock products from real-time correction streams by the Centre National d'Études Spatiales (CNES.³) The latest Global Pressure and Temperature (GPT3) model is used as an a-priori troposphere model [56,59] and the residual ZWD is estimated. In contrast to the PP solution, ZWD and station coordinates are estimated every epoch (30 seconds) using an extended Kalman filter approach. Both solutions follow the findings of Hadas et al. [60], applying an elevation-dependent, cosine-type weighting function with a cutoff angle set to 3°. Atmospheric gradients are estimated every twelve hours. As both solutions represent static PPP processing, station coordinates are tightly constrained to a minimal noise level (low mm-range). During the processing, all missing receiver phase center offsets (PCOs) and phase center variations (PCVs) of Galileo and GLONASS were replaced with GPS L1 values. raPPPid does currently not allow processing over the day-boundary. Thus, each day was processed individually and this strategy was also applied for the PP solution.

2.1.2. Validation: COSMO-1E

As an external reference for tropospheric delay products, we make use of signal delays calculated from the Consortium for Small-scale Modeling (COSMO) model. COSMO is a non-hydrostatic, limited-area

¹ <https://github.com/TUW-VieVS/raPPPid>

² <https://viewswiki.geo.tuwien.ac.at/raPPPid>

³ <http://www.ppp-wizard.net/>

NWP model, which is developed and used by the members of the consortium as well as related institutes and universities. The COSMO-1 model version is operated by MeteoSwiss and operationally run for the entire alpine region on a grid with 1.1 km \times 1.1 km horizontal resolution. Many different data sources are routinely used for data assimilation including radiosonde measurements, aircraft observations, wind profiler measurements as well as radar surface precipitation from the Swiss Radar Network. However, no GNSS data is assimilated operationally into COSMO-1 yet. Therefore, a fully independent validation of GNSS-derived troposphere products is possible. In this study, we make use of output from the ensemble forecast system of COSMO-1 (COSMO-1E, [61]). It comprises an ensemble of eleven forecasts, specifically targeting short-range weather forecasting. Ensemble forecasts up to 33 h ahead are calculated eight times a day for the entire model domain, covering 1075 \times 691 grid points and 80 vertical layers, up to an altitude of 22 km.

In the following, the detailed procedure of ZTD computation, as outlined in Wilgan and Geiger [62], is introduced. Therefore, we utilize the meteorological parameters air pressure p , temperature T and specific humidity q from hourly COSMO-1E analyses (daily at 00UTC) and forecasts (+23 h). In a first step, air pressure and specific humidity fields are utilized to derive water vapor pressure e using:

$$e = q \cdot \frac{p}{(r + (1-r) \cdot q)} \quad (9)$$

where $r = R_d/R_w$ represents the ratio of the dimensionless dry and wet gas constants $R_d = 287.0586$ and $R_w = 461.525$. The total refractivity N_{tot} at each grid point can then be calculated using Eq. (2). ZTD values at a 2D (latitude, longitude) grid are inferred via vertical integration of total refractivity N_{tot} :

$$ZTD_{COSMO} = 10^{-6} \int_{H_{GNSS}}^{H_n} N_{tot} \quad (10)$$

where H_{GNSS} and H_n denote the heights of the GNSS antenna and the COSMO top model level, respectively. The integration over the discrete vertical model levels (from lowest to highest level), for each respective 2D point in the COSMO-1 domain, is approximated using:

$$ZTD_{grid} = 10^{-6} \sum_{i=1}^{n-1} \frac{N_i + N_{i+1}}{2} \cdot \delta s_i \quad (11)$$

where N_i is the total refractivity at the i th vertical level, n is the number of vertical levels of COSMO-1 and δs_i denotes the geometric distance between the i th and the $(i+1)$ -th layer. Furthermore, the delay at and above the top level (n) is derived using Eq. (12) [54]:

$$ZTD_{top} = 0.002277 \cdot (p_n + (\frac{1255}{T_n} + 0.05) \cdot e_n) \quad (12)$$

where p_n , T_n and e_n represent the respective parameters at the highest vertical level of COSMO-1. The total ZTD is then derived by Eq. (13)

$$ZTD_{COSMO} = ZTD_{grid} + ZTD_{top} \quad (13)$$

In this way, an hourly 2D grid of ZTD is produced, from which an interpolation to the respective station position can be carried out. This spatial interpolation is done by an ordinary kriging approach [63], using a gaussian variogram model. A small sub-grid spanning $\pm 0.15^\circ$ in latitude/longitude around the station position is used to do the spatial interpolation of ZTD to the GNSS site. The implementation of this approach is carried out using the PyKriging Python module [64]. For a detailed discussion of the ordinary kriging approach and more general information on kriging we refer to Cressie [65].

2.2. GNSS-IR products: Soil moisture

In addition to troposphere monitoring, the prototype site also offers good conditions for soil moisture retrieval. The area around the stations is sufficiently flat, which is a necessary condition to retrieve unbiased SNR phase estimates. These estimates can then be used for

derivation of soil moisture, in form of volumetric water content (VWC). In order to analyze the performance achievable for soil moisture estimation, three months of GNSS-SNR data are processed with the gnsrefl-software [66], which is an open-source software package for GNSS-IR applications such as soil moisture or snow depth retrieval. The software is available online.⁴ Here, we use the latest beta-version (1.2.9) of the software, which is the first one providing the opportunity to estimate VWC.

The principle of the GNSS-R ground-based soil moisture retrieval was first explained by Chew et al. [44], and is based on the estimation of the phase of a sinusoidal model fitted to the detrended SNR data of a passing satellite, typically at low elevations from around 5 to 25 degrees. The model reads:

$$\text{SNR}(\sin(\theta)) = A \cdot \cos(\omega \cdot \sin(\theta) + \phi) \quad (14)$$

with $\omega = 4\pi h/\lambda$. θ is the topocentric elevation of the satellite, A is the SNR amplitude, ω is the SNR angular frequency, and ϕ the sinusoid phase. A and ϕ are estimated from the SNR data of each individual satellite. For the determination of ω , the wavelength λ of the particular carrier phase signal under investigation has to be inserted. The reflector height h above ground linearly relates to the frequency of the detrended SNR signal, and is determined by means of the Lomb-Scargle periodogram. The algorithm uses the L2C signal, which has shown to have a more precise SNR signal, as a consequence of the new L2C code being more robust than the L1 C/A code [67]. For this reason, we can also use the ZED-F9P for this purpose. At the moment, the computation uses GPS satellites only. By averaging the estimates of different satellites, VWC is provided on a daily basis. The linear relationship between the estimated phase in Eq. (14) and VWC is calculated following the approach of Chew et al. [44]. Beside the conversion to VWC, the software is also capable of applying vegetation corrections, which can significantly impact the estimated phase. The used algorithm for retrieving GPS soil moisture is extensively explained in Chew et al. [46]. After the selection of GPS satellite tracks with clear SNR oscillations, the mean reflector height (for the determination of ω) is estimated and important SNR metrics are computed from Eq. (14) (amplitude A , phase ϕ). After correcting the phase for a phase reference value (*zero* phase, resulting in $\Delta\phi$), the VWC is computed by

$$\text{VWC}_i = S \cdot \Delta\phi + \text{RMC}_i \quad (15)$$

For time series with no significant vegetation, the linear relation between observed phase and soil moisture content can be estimated by $S = 1.48 \text{ cm}^3 \text{ cm}^{-3} \text{ deg}^{-1}$ [44]. The residual moisture content (RMC) is a correction value associated to soil texture, and the gnsrefl software uses a publicly available US Geological Survey dataset to compute the correction [46]. In case the normalized amplitude remains below a certain threshold, a vegetation filter is applied, and Eq. (15) is slightly modified. Fig. 1 shows the observed L2C SNR (“S2”) for the prototype station REH, for four consecutive days in 2022, for the GPS satellite PRN 25. The quantization effects of the observed SNR are typical for u-blox receivers, which provide SNR only as integer values of dB-Hz. However, the long-periodic variations caused by the reflecting surface can still be seen in the curves.

2.2.1. Validation: SwissSMEX

Similar as tropospheric delay products, soil moisture estimates need to be validated by an external data source in order to assess the quality of our solution. Therefore, we utilize in-situ measurements of VWC at REH, which are carried out in the framework of the Swiss Soil Moisture EXperiment (SwissSMEX, [68]). SwissSMEX is a joint project, initiated by ETH Zurich, Agroscope ART, and MeteoSwiss in 2008, with the aim of building a dense network for soil moisture monitoring over Switzerland. The network consists of 19 sites at 17 locations (14

⁴ github.com/kristinemlarsen/gnsrefl

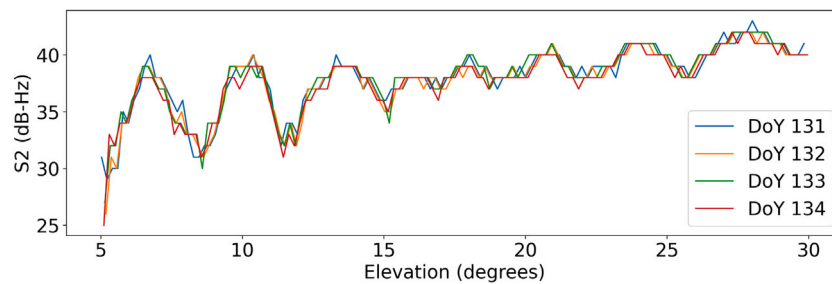


Fig. 1. Observed L2C SNR at station REH for GPS satellite PRN 25, for four consecutive days in 2021..

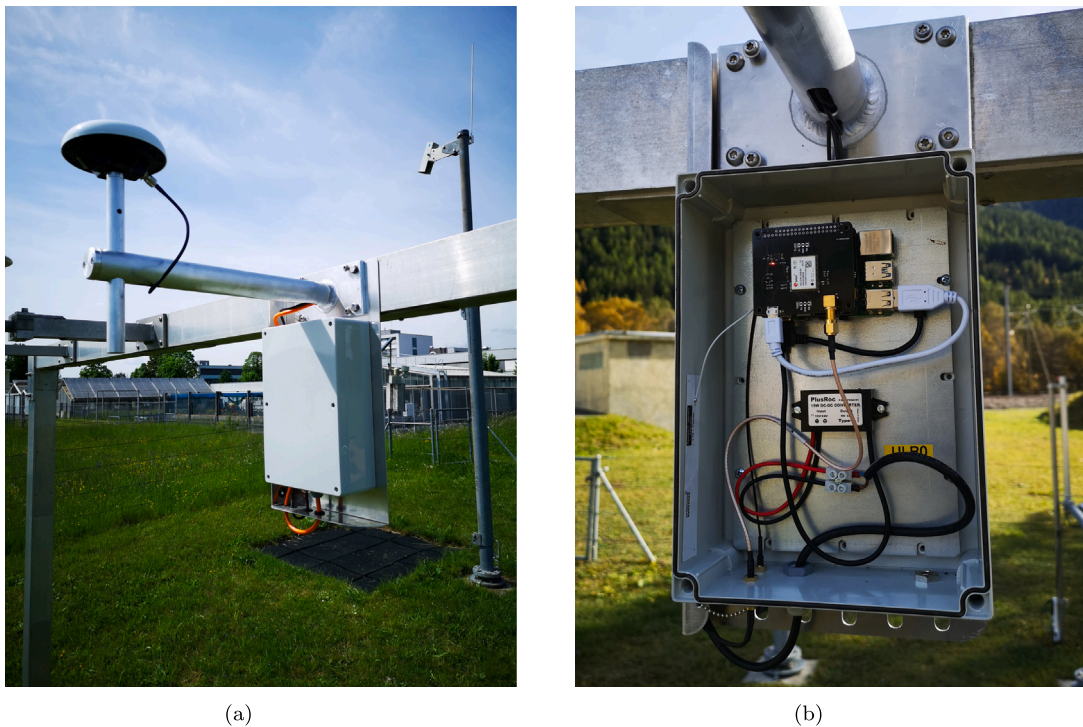


Fig. 2. (a): Full MPG-NET prototype setup installed at REH. (b): Interior of the box containing the main parts of the MPG-NET data logging system.

grassland, 1 arable, and 4 forest stations) and measurements are still ongoing at most locations. More details on the project can be found in Mittelbach and Seneviratne [68] and online.⁵

The WVC observations used in this study are provided for a three-month period (June–August 2022) in form of daily averages, computed from time domain reflectometry measurements taken every ten minutes at 10 cm soil depth. No additional smoothing or other filtering methods are applied to the data.

3. System design and station setup

The following section introduces the station design, in terms of the utilized hardware including the data logging system and the GNSS components. Furthermore, it shows the actual integration of a prototype system at REH. Finally, it also gives an overview of the current state of the network and discuss plans for future sites.

3.1. GNSS data logging system and instrumentation

A dedicated data logging system, fitting to the needs of deployment at meteorological stations, was designed at ETH Zurich specifically for

the project. The mechanical constructions include a measurement arm to be mounted in a similar fashion as already existing sensors at SMN sites. The measurement arm allows for the GNSS antenna to be attached on top of it. This setup can be deployed at the majority of existing SMN station setups and therefore provides flexibility in terms of station selection. The entire data logging system and GNSS payload utilized for the project consists of the following components:

- **Raspberry Pi 4:** The Raspberry Pi 4 serves as the data logging and transfer system. Binary GNSS raw data are stored and transferred to an internal server via File Transfer Protocol (FTP).
- **Long Term Evolution (LTE) Modem:** The modem is required to establish an internet connection for the FTP transfer.
- **u-blox ZED-F9P multi-GNSS receiver module:** The receiver module, in combination with the GNSS antenna, is responsible for collecting raw GNSS observations. It is connected to the Raspberry Pi via a Universal Serial Bus (USB) port.
- **GNSS antenna:** Two different types of low-cost helix antennas are used for different stations in the network, which are described in Table 2. Both of them are capable of logging multi-GNSS, DF observations, but are significantly different in price, as Table 2 shows.

⁵ iac.ethz.ch/group/land-climate-dynamics/research/swissmex.html

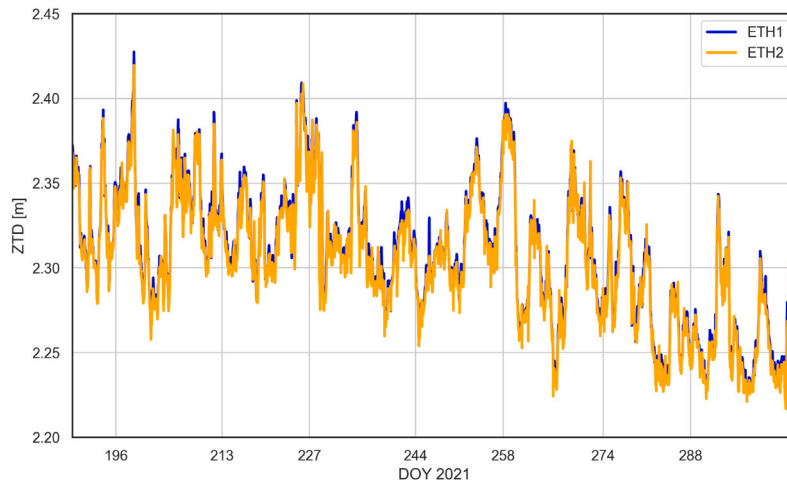


Fig. 3. Comparison of ZTD estimates between our low-cost payload setup ETH1 (blue) and the geodetic-grade payload of AGNES station ETH2 (orange). Observations were gathered between DOY 194-300 of 2021 at the rooftop of ETHZ.

Table 2

Payload solutions investigated in the course of this study. POLANT refers to the Septentrio PolaNt* MC antenna and ASANT to the ArduSimple “survey” AS-ANT2B-CAL antenna.

| Payload name | Receiver | Antenna | Price [CHF] |
|--------------|----------------|------------------|-------------|
| ETH1 | u-blox ZED-F9P | POLANT | ~1400 |
| ETH2 | TRIMBLE NETR9 | TRIMBLE TRM59800 | ~20000 |
| ETH3 | u-blox ZED-F9P | ASANT | ~600 |

Fig. 2(a) shows the installed setup at the prototype site REH and (b) provides a look at the data logging system deployed at the newly-installed MPG-NET station at Ulrichen (see Fig. 5).

3.2. GNSS sensor station

As the main influence on the quality of derived results and products, the GNSS instrumentation is the key component of the station setup. As already mentioned in the introduction, the term low-cost GNSS is not restricted to solely single-frequency GNSS equipment anymore. Therefore, single-frequency solutions already existing at ETH Zurich before the initiation of MPG-NET, were also upgraded to DF capabilities. This DF upgrade was achieved by incorporating the u-blox ZED-F9P GNSS receiver module into our data logging system. The quality of its solution for different purposes has been proven in a number of studies, most of them already mentioned in the introduction. Nevertheless, we still investigated and cross-compared different hardware solutions in the course of the MPG-NET station design development. An overview of the solutions utilized in these performance tests is given in Table 2.

In order to make use of DF capabilities, also the GNSS antenna needs to be chosen adequately. Initial tests using different antenna types showed the importance of the utilized antenna, e.g. for tropospheric estimation, and thus confirm findings of other studies [36]. Originally, the payload ETH1 using the Septentrio PolaNt* MC (termed POLANT in the following), was chosen for the MPG-NET setup. The antenna was tested over a period of over three months (116 days) in 2021 on the rooftop of the ETH building, with coordinate and troposphere estimations showing very promising results in comparison to geodetic-grade equipment of the ETH2 station (payload ETH2 in Table 2) of the Automated GNSS Network Switzerland (AGNES). The comparison of the ZTD estimates from both stations is shown in Fig. 3 and respective statistics are provided in the first column (ETH1-ETH2) of Table 3. Both station setups are only a few meters away from each other and have a height difference of about five meters, which has been corrected for the ZTD estimates shown (results refer to the height of ETH1). Results

Table 3

Calculated are bias, standard deviation (SD), root mean square (RMS) error (all in [mm]) and Pearson correlation coefficient (R) of the ZTD comparison. Please note the differing analysis periods for results shown in column one (ETH1-ETH2, three months) and two (ETH1-ETH3, about 36 h in total).

| | ETH1-ETH2 | ETH1-ETH3 |
|-----------|-----------|-----------|
| Bias [mm] | 3.3 | -2.2 |
| SD [mm] | 3.7 | 2.2 |
| RMS [mm] | 4.9 | 3.2 |
| R | 0.97 | 0.96 |

show very low bias, standard deviation and RMS (2–3 mm) and a very high correlation of 0.97. Thus, we conclude that the performance of our payload is comparable to the geodetic-grade setup used for AGNES stations.

Therefore, we initially chose this antenna for the MPG-NET prototype station in Zurich-Affoltern (see Section 3.3).

However, with the rapid advancements in GNSS hardware, even cheaper antenna types (promising comparable accuracy) became available in the meantime. One of these antenna types is the helical-type low-cost antenna ArduSimple “survey” AS-ANT2B-CAL (termed ASANT in the following). Its performance for kinematic PPP applications (such as rapid ground movements) was recently investigated in Hohensinn et al. [23]. It showed very promising results, while coming at about a tenth of the price of the POLANT. For these reasons, we decided to test an additional setup using the ZED-F9P in combination with this antenna (ETH3) by comparing its results to those of ETH1. In order to show their comparability, Fig. 4 and the second column of Table 3 present the results of the ZTD comparison between ETH1 and ETH3. Data stems from an experiment conducted for several hours during the period 23.-24.03.2022 on the ETH rooftop. Results again show very small error statistics and a high correlation for the analyzed (not continuous) three time periods of approximately 36 h in total. Only one of those periods is shown in Fig. 4. The results indicate that the performance of the ETH3 setup is comparable to ETH1 for ZTD retrieval. Thus, it was decided to deploy the ETH3 setup at the other MPG-NET sites in the future.

3.3. Prototype site Zurich-Affoltern

In order to initially test the station setup (here still the ETH1 setup), a prototype solution was installed at REH in May 2022. The main reason for choosing this site for prototype deployment is the obvious advantage of its location in the vicinity of ETH Zurich. This allows

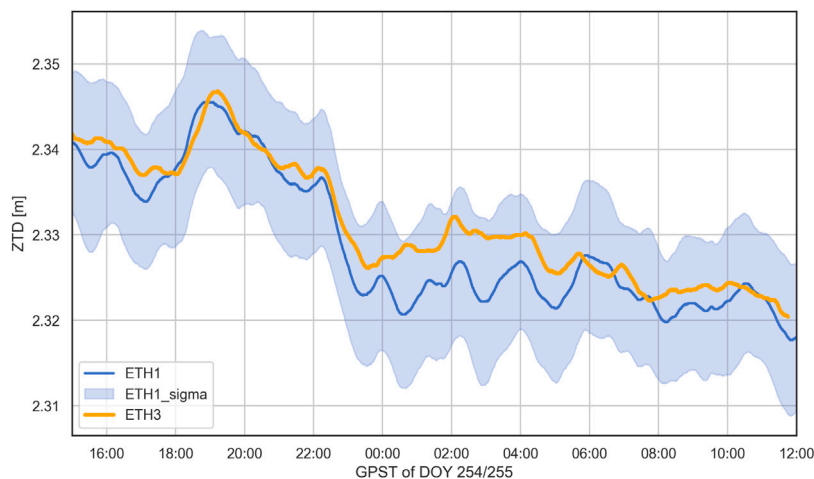


Fig. 4. Comparison of ZTD estimates of the antenna setups ETH1 (POLANT, blue) and ETH3 (ASANT, orange). In addition, the formal standard deviation of ETH1 is indicated by the blue-shaded area. Observations were gathered on day of the year (DOY) 254 and 255 of 2022 at the rooftop of ETH Zurich.

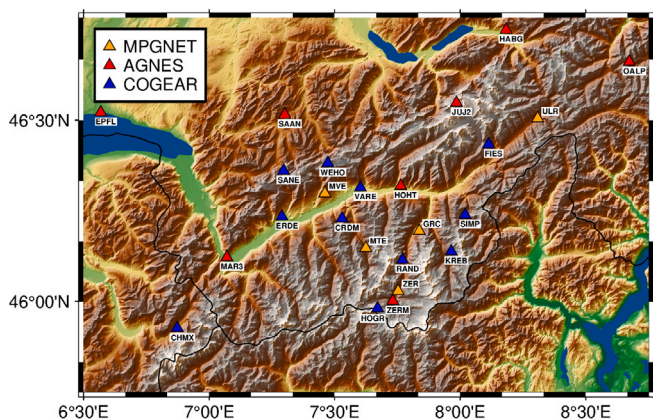


Fig. 5. Already existing MPG-NET stations and additional GNSS station infrastructure in the Valais area.

for easy access and troubleshooting in a minimal amount of time. Furthermore, the site also offers good prerequisites for soil moisture retrieval because of the flat grassland surrounding it. Finally, also other research groups conduct soil moisture measurements there (see Section 2.2.1), which gives the unique opportunity of cross-validation on-site. The realization of our setup is visualized in Fig. 2(a).

3.4. Current status of the station network

At the moment, MPG-NET already consists of seven stations, five of them located in the Valais area, one in Graubünden and the prototype site at Zurich-Affoltern. Fig. 5 presents a topographic map of the Valais area with the existing GNSS infrastructure in the region. In general, GNSS stations from three different networks are available:

- MPG-NET
- AGNES
- The Coupled Seismogenic Geohazards in Alpine Regions (COGEAR) network (also operated by ETH Zurich)

The five stations of MPG-NET shown in Fig. 5 (orange triangles) have been set up at the respective SMN sites Graechen (GRC), Montana (MVE), Mottec (MTE) and Ulrichen (ULR). Furthermore, one additional station (Weissfluhjoch, WFJ) has recently been installed in the Graubünden area. Table A.5 in Appendix gives an overview of all planned and already operating MPG-NET stations.

4. Results: Zurich-Affoltern

As a first performance assessment of the MPG-NET station setup, we show initial results for the prototype installation of the introduced payload at REH in the following section. Two types of products mentioned in Section 2, ZTD and VWC were generated for the first three months of operation. Results for these two product types are presented in the following Sections 4.1 and 4.2.

4.1. Tropospheric delays

As a first product from the prototype site REH, we show time series of ZTD for the time period 01.06.-01.09.2022 in the following sections. Specifically, the performance of ZTD solutions calculated with different software packages and latencies (Table 1) is investigated. Furthermore, we assess the quality of ZTD products by an external validation using ZTD calculated from COSMO-1.

4.1.1. Comparison of final and real-time ZTD products

For a first performance and consistency assessment, we compare the PP- and RT-ZTD solutions. For this comparison of epoch-wise RT-ZTD with hourly PP-ZTD estimates, we average both solutions over 30 min, which represents a suitable interval for future NWP applications, such as nowcasting.

Fig. 6 shows the RT-ZTD and PP-ZTD solution in green and red, respectively. The direct comparison reveals a very high agreement and correlation between the solutions. Additionally, Fig. 6 shows precipitation events observed at the prototype site. As expected, both ZTD solutions are able to capture the major precipitation events observed. Table 4 presents common statistical error measures for this comparison. The bias, standard deviation, and root-mean square (RMS) error of the solution differences are at the mm — low cm level on average. Still, the RT solution shows a significantly higher noise, which is reasonable considering the epoch-wise parameter estimation carried out, even when averaging over 30 min. Fig. 7 presents the bias and standard deviation for each day, except DOY 187, which is not available in the RT solution due to missing correction streams. For most days of the analyzed period, the bias and the standard deviation are between 5–10 mm, which indicates a good performance of the RT-ZTD solution compared the PP results.

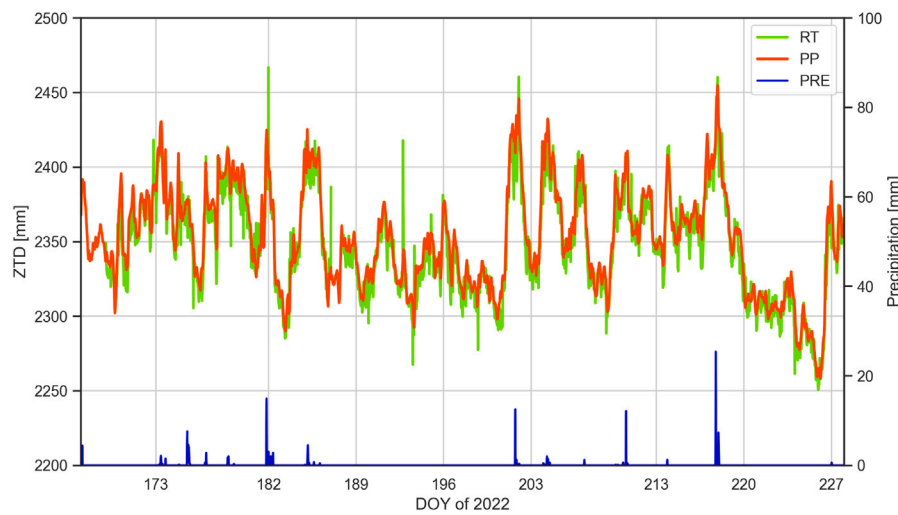


Fig. 6. Comparison of the RT (green) and PP (orange) ZTD solutions for the period 01.06.–01.09.2022 at the prototype site REH. Additionally, precipitation events observed during that period are shown in blue.

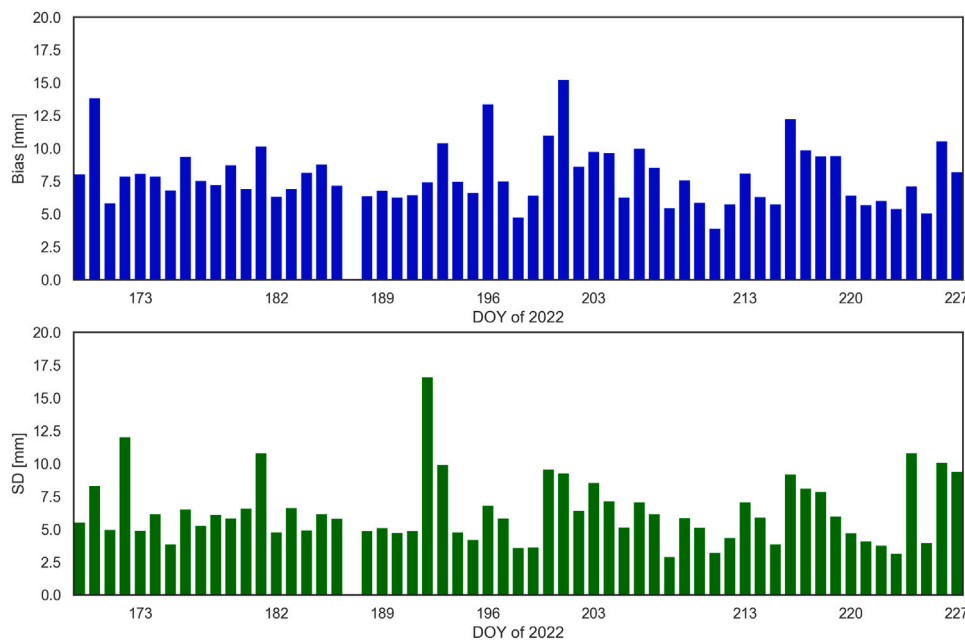


Fig. 7. Daily results for ZTD bias (top, blue) and standard deviation (bottom, green) for the RT-PP product comparison shown in Fig. 6.

Table 4

Overview of statistical measures calculated for the cross-validation between PP- and RT-ZTD products as well as external validation of both products against COSMO-1. Calculated are bias, standard deviation (SD), root mean square (RMS) error (all in [mm]) and Pearson correlation coefficient (R). Please note that the time span analyzed for columns two and three is 01-21.07.2022 and therefore different from results shown in column one (15.6-15.8.2022).

| | PP-RT | PP-COSMO | RT-COSMO |
|-----------|-------|----------|----------|
| Bias [mm] | 5.1 | -10.4 | -13.6 |
| SD [mm] | 9.3 | 13.4 | 19.4 |
| RMS [mm] | 10.6 | 16.9 | 23.7 |
| R | 0.97 | 0.92 | 0.83 |

4.1.2. Validation using ray-traced ZTD

In addition to the cross-comparison between PP- and RT-ZTD products, we carry out an independent validation using ZTD computed from

COSMO-1 data. The COSMO-1 model and the ray-tracing algorithm used for ZTD computation have been introduced in Section 2.1.2.

Fig. 8 shows the comparison of COSMO-1-derived ZTD (NWP-ZTD) with PP- and RT-ZTD for a three-week period in July 2022 (01-21.07.2022). Respective statistics are given in the second and third column of Table 4. Due to COSMO-1 data availability, this validation period is shorter than the two-month PP-RT comparison period (Figs. 6 and 7). We plan to use longer COSMO-1E time series for future validation campaigns. Overall, results reveal a good agreement between the ray-traced ZTD and the GNSS-derived solutions. Nevertheless, distinctive biases (10–13 mm) and standard deviations (13–19 mm) are still present for both GNSS ZTD solutions. The bias values are reasonable and compliant with current accuracy requirements for NWP data assimilation (< 15 mm). Moreover, it should be noted that evident biases might still be mitigated in NWP pre-processing, which typically involves a bias correction of assimilated observations against the model background. The PP solution shows a standard deviation compliant with accuracy standards, but the RT solution currently exceeds the

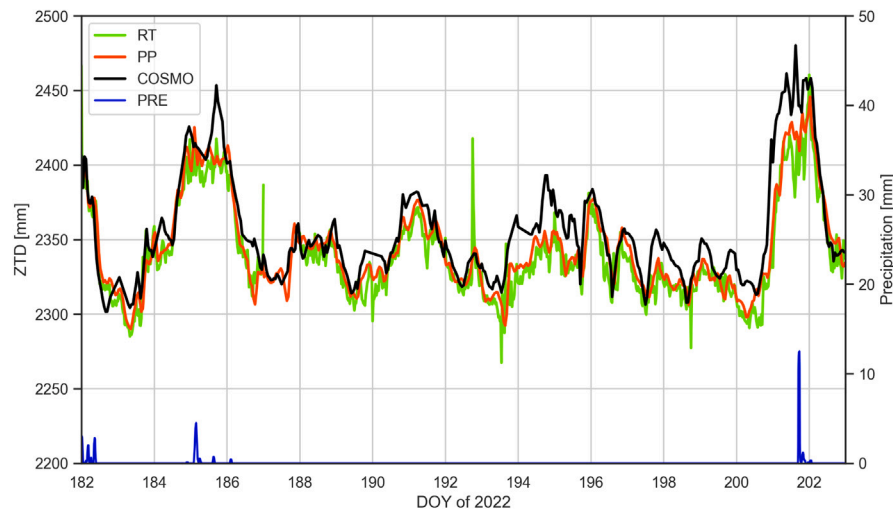


Fig. 8. Comparison of the RT (green) and PP (orange) ZTD solutions with ray-traced ZTD from COSMO-1 (black) for the period 01.07.–07.07.2022 at the prototype site REH. In addition, precipitation events (PRE) are indicated in blue.

limits. Several reasons for this are conceivable, from GNSS processing strategies to possible uncertainties present in the COSMO-1 model. In terms of GNSS processing, e.g. the fact that currently no antenna phase center corrections are available for POLANT might introduce errors in the mm-range to the GNSS solutions. Furthermore, we currently use only one COSMO-1 analysis per day (00 UTC) and compute the other 23 h from forecast data, which might introduce additional uncertainty to the ray-traced ZTD. For some periods which show larger deviations between the solutions, these deviations are increasingly present in the later hours of the respective days (e.g. DOY 185), which is compliant with the supposition stated above. Therefore, we plan to make use of all analyses available per day (one every three hours) in future evaluations.

4.2. Volumetric water content

Besides the estimation of tropospheric delays, the prototype site also provides good conditions for soil moisture retrieval, as the surrounding area is flat grassland. Moreover, it provides an unique opportunity for external validation of our VWC estimates, since it is part of the SwissSMEX (see Section 2.2.1). As for the troposphere products, three months of L2C observations have been processed with the `gnssrefl` software. Fig. 9 shows a summary of Lomb-scale periodograms derived for GPS L2C SNR observations of DOY 200 for all four quadrants. The periodograms depict the spectral density of estimated reflector heights. These types of plots are the default output of the `quickLook` option of `gnssrefl`. They provide a helpful tool for an initial assessment of the station's suitability, by giving a good indication if a planar reflector surface is present below your antenna. Different colors show reflector height retrievals from different satellites, and gray lines indicate failed retrievals. Considering the fact that the real reflector height at REH is approximately 2.1 m, it becomes evident that reasonable results for VWC estimation can only be obtained in the southeast direction. This finding is consistent with the station setup and its surroundings, as most other directions are obstructed by other measurement equipment. Therefore, the results presented in Fig. 10 represent VWC estimates for southeast directions, which (by coincidence) is also the direction where the validation measurements from SwissSMEX are carried out.

In the following, we use the new soil moisture module of `gnssrefl` for VWC estimation. This module utilizes phase estimations instead of reflector heights [44], which have to be computed for the entire period. VWC is inferred from these phase estimations, and a vegetation correction [46] is applied. For this initial assessment we use the default settings of `gnssrefl`, but in the future, further tuning of the processing

settings will be investigated. Vegetation-corrected VWC is obtained for the analyzed period and the results are shown in Fig. 10. In general, the results are very promising as the main trends observed in GPS estimates (VWC_GPS) are consistent with the reference data set (denoted as VWC_TD_010). However, there are also some distinctive differences between the results from both sensors. There is a significant bias, reaching up to 10%, as well as a small time lag present between the time series of both sensors. Furthermore, the variability of the GPS estimates is much higher than for the in-situ measurements. All of these facts can be partially attributed to the sensors differing observation characteristics, predominantly the representative measurement (soil) depth. The following section discusses these differences and their effects on the validation results in greater detail.

5. Discussion

In the previous section some initial results from the MPG-NET prototype setup at REH have been shown. In this section, we discuss the findings from these results for the two analyzed product types in more detail.

- 1. Tropospheric delays:** As already expected from the sensor test campaigns, the chosen setup is able to deliver high-quality troposphere products, which comply with standards of possible use scenarios, such as data assimilation in NWP. Validation of PP-ZTD solutions shows a bias and standard deviation of 10/13 mm against NWP-ZTD respectively (Fig. 8). Therefore, they are able to meet typical accuracy requirements for NWP applications. Consistency between PP- and RT-ZTD solutions is high (Figs. 6 and 7) and RT-ZTD results are comparable with performance levels reported in recent studies [69].

For the external validation against NWP-derived ZTD (Fig. 8), the RT-ZTD solution currently shows a slightly larger bias and standard deviation compared to the PP solution (13/19 mm respectively). Thus, some advancements in the RT processing scheme and software are still necessary, but results are expected to improve with e.g. future usage of antenna phase center corrections, which are not available yet. Furthermore, the validation results also contain some uncertainty on the level of reference data (COSMO-1E), as mostly forecast data has been utilized in this initial assessment. We plan on only using COSMO-1E analysis fields for future validation efforts.

In comparison with the results presented by Marut et al. [38] for similar low-cost GNSS instrumentation, we find equivalent

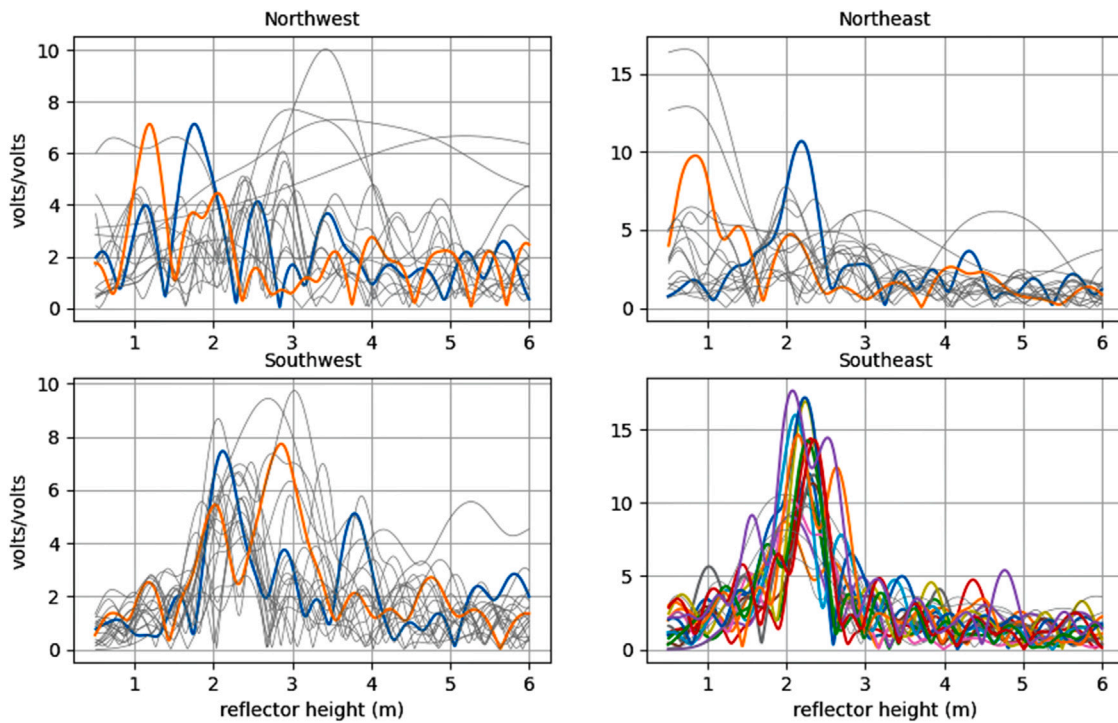


Fig. 9. Lomb-scale periodograms of reflector heights for different quadrants around the prototype site REH, as computed and visualized by the QuickLook option of gnsrefl. Different colors represent different GPS satellites used to retrieve reflector height.

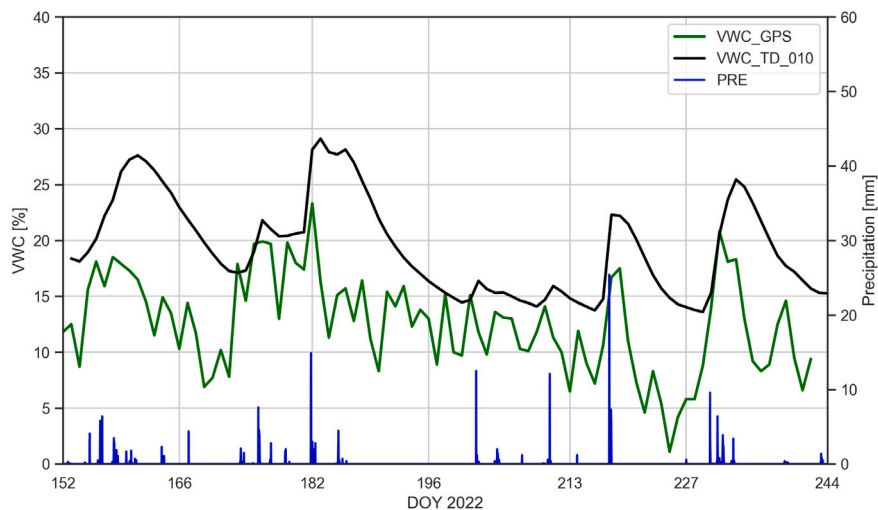


Fig. 10. Time series of VWC at prototype site REH, derived from GPS-SNR (VWC_GPS, green) and the SwissSMEX in-situ soil moisture sensor (VWC_TD_10, black) for the period of 01.06–01.09.2022. In addition, precipitation amounts measured at the site are visualized in blue.

accuracy levels in terms of bias and standard deviation when comparing low-cost ZTD results with geodetic-grade instrumentation. For the validation using external reference data, slightly higher standard deviations and biases were found for our station setup. However, it should be noted that two factors complicate this comparison. First, Marut et al. [38] carried out this external validation on the level of IWV, which makes a direct comparison difficult. In order to relate their IWV error statistics to our ZTD results, we used uncertainty propagation for IWV as proposed in Ning et al. [70]. Secondly, they used a different type of reference data, a water vapor radiometer located only a few meters away from their GNSS setup, in contrast to NWP data which needs to be interpolated to the station location. Nevertheless, we will also provide IWV products from MPG-NET in the future

and plan to carry out further comparisons with their results in the future.

2. **Soil moisture:** In addition to tropospheric delays, also products from GNSS-IR can be retrieved from MPG-NET stations. In this study, we focused on presenting initial results for soil moisture (i.e VWC) estimation from GPS signals at the prototype site Zurich-Affoltern. GNSS-IR VWC estimates show reasonable levels and a high sensitivity to precipitation events recorded at the site. However, problems exist for extended dry periods which still show a significant amount of variability in the absence of precipitation. Cross-validation of estimates from the first months using reference data from SwissSMEX revealed high levels of agreement between GPS and the reference sensor, especially in terms of correlation and temporal evolution of soil moisture

levels. Nevertheless, some distinctive discrepancies are also evident. As outlined in Section 4.2, a significant bias of up to 10% between the results from GPS and in-situ sensors is observed. Furthermore, a small time lag between the time series is apparent and GPS estimates show much larger variability compared to in-situ measurements. However, all of these facts can largely be explained the differing measurement characteristics of both sensors, most importantly the soil depths for which the sensors measurements are representative.

First of all, in-situ measurements are taken at 10 cm soil depth, whereas GPS estimates are representing VWC in the layer nearest to the surface. That is why GPS estimates are typically compared with reference sensors in 5 cm or even smaller soil depths. Unfortunately, no such near-surface sensor was operating during the time period analyzed in this study. Lower soil layers tend to have higher VWC levels, a phenomenon which is even more pronounced during long dry periods. Such a period was observed in summer 2022 (visible from Fig. 10 between DOY 185–200). These facts might explain a certain proportion of the observed bias. Furthermore, small-scale soil heterogeneity is known to have a large influence on absolute VWC values (see e.g. [71]), which is why typically analyses focus on temporal variability of VWC rather than its absolute values [68]. At last, some level of bias might be introduced by GNSS-IR related problems such as calibration effects (e.g., vegetation correction), which we aim to further investigate in future studies.

The differing reference depths also explain the slight time lag which can be observed between the main peaks of VWC_TD_010 and VWC_GPS as well as those of VWC_TD_010 with observed precipitation amounts. An obvious reason for this behavior is the longer time period it takes for moisture to penetrate to greater soil depths.

Finally, the higher variability in GPS VWC estimates can also be related the smaller penetration depth of the GPS signals, as the variability in the top layers is generally higher and precipitation signals are increasingly smoothed out as moisture penetrates to greater soil depths. In addition, the GNSS-IR measurement principle might also account for a higher variability (in terms of noise level), especially when small numbers of usable satellite tracks can be observed.

Nevertheless, these initial results already show very promising performance of the current station setup.

6. Conclusions and future plans

In this study, we introduced the idea, conceptualization and realization of the low-cost GNSS co-location station design, to be used within the multi-purpose GNSS network MPG-NET. MPG-NET was initiated by the chair of Mathematical and Physical Geodesy, in the course of a pilot project in cooperation with MeteoSwiss. In the future, the network will be maintained by the new chair of Space Geodesy at ETH Zurich.

The introduced GNSS data logging system is based on a Raspberry Pi 4, to which an LTE modem for data transfer and the ZED-F9P GNSS chipset are attached. The ZED-F9P is connected to a low-cost helix antenna, capable of logging multi-GNSS, dual-frequency observations. Two different types of antennas were tested and subsequently used for MPG-NET stations. The entire logging system is attached to a specifically designed measurement arm, fitting to the requirements of SMN stations, and thus is easy to install at the majority of SMN sites.

The performance of the station setup and payload was shown by presenting initial results from the prototype site Zurich-Affoltern during the first months of operation. Specifically, results for two products types, tropospheric delays and soil moisture estimates have been discussed. Results for post-processed ZTD products show that the chosen setup is able to deliver high-quality products, which comply with standards of possible use scenarios, such as data assimilation in NWP.

Real-time products are highly consistent with post-processing solutions, but external validation with NWP data shows that some improvements in terms of software and processing strategy are still needed. In general, these first results are promising and the use-cases of MPG-NET troposphere products are manifold. While post-processed ZTD products are an interesting observation for model validation and long-term climate studies, real-time ZTD can be used for NWP-based nowcasting, providing improvements for the prediction of severe weather events.

As an additional product, soil moisture estimates were produced at REH for a period of three months over the summer of 2022. The results, obtained from an initial processing effort using the gnss-refl software, are promising as well. Cross-validation of VWC estimates from the first months using reference data from SwissSMEX revealed high levels of agreement between GPS estimates and the reference sensor, especially in terms of correlation and temporal evolution of soil moisture levels. Still, some reasonable discrepancies, related mostly to the difference in penetration depth of GPS signals (below 5 cm) compared to the reference measurements (10 cm), are evident. Nevertheless, these initial results already show very promising performance. Therefore, we aim to extend the VWC estimation to other suitable stations in the network and plan to conduct a detailed feasibility analysis for each MPG-NET site.

The MPG-NET project is still in progress. Up to this point, seven of the planned ten stations are operating and the remaining three are expected to be installed in early 2023. Beside the installation of the remaining stations, a non-exhaustive list of future plans for MPG-NET also includes the following points:

- Processing routines and product generation will be continued for the prototype station shown in this study and extended to the whole existing (and still planned) stations. We plan to also establish a near real-time solution using the respective orbit and clock products and incorporate in-situ pressure observations for accurate modeling of ZHD.
- We might test low-cost equipment from other manufacturers and compare its performance to our current station setup.
- New products will be derived from already existing and future stations. These include snow-related parameters such as snow height and snow-water-equivalent as well as coordinate time series, especially in seismically active regions such as the Valais area. In terms of troposphere products, plans include the provision of IWV by making use of in-situ temperature and pressure measurements for the conversion from ZTD as well as ZTD maps produced by spatial interpolation of dense GNSS networks (e.g. in the Valais area).
- We are currently setting up a dedicated database for GNSS-derived products, the GNSS Monitoring Center (GMC.⁶) GMC includes products from MPG-NET, COGEAR and other networks of monitoring stations operated by ETH Zurich. The aim is to provide a multitude of high-quality products for environmental monitoring and make them available to a broad scientific community.
- An overall goal of the project will be the development of an integrated monitoring approach that combines the different product types for the monitoring of natural hazards such as landslides, extreme precipitation events or floods. As many of these hazards result from a combination of multiple processes, monitoring not only the impact (e.g. deformation seen in coordinate time series) but also parameters related to possible trigger mechanisms (water vapor, soil moisture) will be beneficial. Such future early-warning systems might fuse different data sets provided by GNSS stations using classical statistical methods as well as data-driven (machine-learning based) approaches.

⁶ accessible via gmc.ethz.ch

Table A.5

Full list of GNSS stations operated/planned for MPG-NET. Indicated are name, geographical location (longitude, latitude and height) as well as the operational status of the respective station.

| Name | Longitude [°] | Latitude [°] | Height [masl] | Status |
|------------------------|----------------|---------------|---------------|---------|
| Arosa (ARO) | 46.792661 | 9.679014 | 1878 | Planned |
| Graechen (GRC) | 46.195314 | 7.836822 | 1605 | Active |
| Montana (MVE) | 46.298806 | 7.460814 | 1423 | Active |
| Mottec (MTE) | 46.147897 | 7.624033 | 1580 | Active |
| Scuol (SCU) | 46.793275 | 10.283267 | 1304 | Planned |
| Sta. Maria (SMM) | 46.602256 | 10.426314 | 1386 | Planned |
| Ulrichen (ULR) | 46.504881 | 8.308236 | 1346 | Active |
| Weissfluhjoch (WFJ) | 46.833325 | 9.806394 | 2691 | Active |
| Zermatt (ZER) | 46.029272 | 7.752433 | 1638 | Active |
| Zurich-Affoltern (REH) | 47.427694 | 8.517953 | 444 | Active |

CRedit authorship contribution statement

Matthias Aichinger-Rosenberger: Conceptualization, Methodology, Data curation, Formal analysis, Visualization, Validation, Project administration, Writing – original draft. **Alexander Wolf:** Methodology, Investigation, Data curation. **Cornelius Senn:** Methodology, Investigation, Data curation. **Roland Hohensinn:** Conceptualization, Formal analysis, Writing – original draft, Visualization. **Marcus Franz Glaner:** Software, Writing – review & editing. **Gregor Moeller:** Conceptualization, Writing – review & editing. **Benedikt Soja:** Supervision, Project administration, Funding acquisition, Writing – review & editing. **Markus Rothacher:** Conceptualization, Supervision, Funding acquisition, Writing – review & editing.

Declaration of competing interest

The authors declare that they have no known competing financial interests or personal relationships that could have appeared to influence the work reported in this paper.

Data availability

Data products from the MPG-NET stations will be made available via our dedicated web portal <https://gmc.ethz.ch> in the future.

Acknowledgments

The authors would like to thank MeteoSwiss for the support in the setup of MPG-NET, providing the opportunity for this (and future) studies, as well as for the provision of COSMO-1 forecast and analysis data for validation purposes. We also thank swisstopo for providing GNSS observations from AGNES station ETH2. Furthermore, we thank the Land-Climate Dynamics group of the Institute for Atmospheric and Climate Science (IAC) at ETH Zurich for providing SwissSMEX in-situ measurements of VWC at Zurich-Affoltern for validation.

Appendix. Station list

See [Table A.5](#).

References

- [1] P.J. Teunissen, O. Montenbruck, *Springer Handbook of Global Navigation Satellite Systems*, Vol. 10, Springer, 2017.
- [2] Y. Bock, S. Wdowinski, GNSS geodesy in geophysics, natural hazards, climate, and the environment, in: *Position, Navigation, and Timing Technologies in the 21st Century: Integrated Satellite Navigation, Sensor Systems, and Civil Applications*, Vol. 1, Wiley Online Library, 2020, pp. 741–820.
- [3] S. Jin, E. Cardellach, F. Xie, *GNSS Remote Sensing*, Vol. 16, Springer, 2014.
- [4] X. Li, F. Zus, C. Lu, G. Dick, T. Ning, M. Ge, J. Wickert, H. Schuh, Retrieving of atmospheric parameters from multi-GNSS in real time: Validation with water vapor radiometer and numerical weather model, *J. Geophys. Res.* 120 (14) (2015) 7189–7204.
- [5] Y. Bock, D. Melgar, Physical applications of GPS geodesy: A review, *Rep. Progr. Phys.* 79 (10) (2016) 106801.
- [6] G. Guerova, J. Jones, J. Douša, G. Dick, S. de Haan, E. Pottiaux, O. Bock, R. Pacione, G. Elgered, H. Vedel, et al., Review of the state of the art and future prospects of the ground-based GNSS meteorology in Europe, *Atmos. Meas. Tech.* 9 (11) (2016) 5385–5406.
- [7] A.M. White, W.P. Gardner, A.A. Borsa, D.F. Argus, H.R. Martens, A review of GNSS/GPS in hydrogeodesy: Hydrologic loading applications and their implications for water resource research, *Water Resour. Res.* 58 (7) (2022) e2022WR032078.
- [8] T. Herring, R. King, S. McClusky, et al., *Introduction to gamit/globk*, Massachusetts Institute of Technology, Cambridge, Massachusetts, 2010.
- [9] R. Dach, S. Lutz, P. Walsler, P. Friedz, *Bernese GNSS Software Version 5.2*, 2015, <http://dx.doi.org/10.7892/boris.72297>.
- [10] J. Zumbege, M. Heflin, D. Jefferson, M. Watkins, F. Webb, Precise point positioning for the efficient and robust analysis of GPS data from large networks, *J. Geophys. Res.* 102 (1997) <http://dx.doi.org/10.1029/96JB03860>.
- [11] J. Kouba, P. Héroux, Precise point positioning using IGS orbit and clock products, *GPS Solut.* 5 (2001) 12–28, <http://dx.doi.org/10.1007/PL00012883>.
- [12] M. Glaner, R. Weber, PPP with integer ambiguity resolution for GPS and Galileo using satellite products from different analysis centers, *GPS Solut.* 25 (3) (2021) 1–13.
- [13] J. Geng, F.N. Teferle, X. Meng, A. Dodson, Towards PPP-RTK: Ambiguity resolution in real-time precise point positioning, *Adv. Space Res.* 47 (10) (2011) 1664–1673.
- [14] J. Geng, X. Chen, Y. Pan, S. Mao, C. Li, J. Zhou, K. Zhang, PRIDE PPP-AR: an open-source software for GPS PPP ambiguity resolution, *GPS Solut.* 23 (4) (2019) 1–10.
- [15] T. Takasu, A. Yasuda, Development of the low-cost RTK-GPS receiver with an open source program package RTKLIB, in: *International Symposium on GPS/GNSS*, 2009.
- [16] C. Roesler, K.M. Larson, Software tools for GNSS interferometric reflectometry (GNSS-IR), *GPS Solut.* 22 (3) (2018) 1–10.
- [17] N. Joubert, T.G. Reid, F. Noble, Developments in modern GNSS and its impact on autonomous vehicle architectures, in: *2020 IEEE Intelligent Vehicles Symposium, IV, IEEE*, 2020, pp. 2029–2036.
- [18] W. Stempfhuber, M. Buchholz, A precise, low-cost RTK GNSS system for UAV applications, in: *Proc. of Unmanned Aerial Vehicle in Geomatics, ISPRS*, 2011.
- [19] J. Paziewski, Recent advances and perspectives for positioning and applications with smartphone GNSS observations, *Meas. Sci. Technol.* 31 (9) (2020) 091001.
- [20] L. Poluzzi, L. Tavasci, F. Corsini, M. Barbarella, S. Gandolfi, Low-cost GNSS sensors for monitoring applications, *Appl. Geomat.* 12 (1) (2020) 35–44.
- [21] P. Limpach, A. Geiger, H. Raetz, Gns for deformation and geohazard monitoring in the Swiss alps, in: *Proceedings of the 3rd Joint International Symposium on Deformation Monitoring*, Vol. 30, JISDM 2016, Vienna, Austria, 2016.
- [22] V. Hamza, B. Stopar, O. Sterle, Testing the performance of multi-frequency low-cost GNSS receivers and antennas, *Sensors* 21 (6) (2021) 2029.
- [23] R. Hohensinn, R. Stauffer, M.F. Glaner, I.D. Herrera Pinzón, E. Vuadens, Y. Rossi, J. Clinton, M. Rothacher, Low-cost GNSS and real-time PPP: Assessing the precision of the u-blox ZED-F9P for kinematic monitoring applications, *Remote Sens.* 14 (20) (2022) <http://dx.doi.org/10.3390/rs14205100>.
- [24] M.S. Garrido-Carretero, M.J. Borque-Arancón, A.M. Ruiz-Armenteros, R. Moreno-Guerrero, A.J. Gil-Cruz, et al., Low-cost GNSS receiver in RTK positioning under the standard ISO-17123-8: A feasible option in geomatics, *Measurement* 137 (2019) 168–178.
- [25] M. Tsakiri, A. Sioulis, G. Piniotis, Compliance of low-cost, single-frequency GNSS receivers to standards consistent with ISO for control surveying, *Int. J. Metrol. Qual. Eng.* 8 (2017) 11.
- [26] T. Takasu, A. Yasuda, Evaluation of RTK-GPS performance with low-cost single-frequency GPS receivers, in: *Proceedings of International Symposium on GPS/GNSS*, 2008, pp. 852–861.
- [27] J. Glabsch, O. Heunecke, S. Schuhbäck, Monitoring the Hornberg landslide using a recently developed low cost GNSS sensor network, *Walter de Gruyter GmbH & Co. KG*, 2009.
- [28] N. Wielgocka, T. Hadas, A. Kaczmarek, G. Marut, Feasibility of using low-cost dual-frequency GNSS receivers for land surveying, *Sensors* 21 (6) (2021) 1956.
- [29] V. Hamza, B. Stopar, T. Ambrožič, O. Sterle, Performance evaluation of low-cost multi-frequency GNSS receivers and antennas for displacement detection, *Appl. Sci.* 11 (14) (2021) 6666.
- [30] S. Dan, A. Santra, S. Mahato, C. Koley, P. Banerjee, A. Bose, On use of low cost, compact GNSS receiver modules for ionosphere monitoring, *Radio Sci.* 56 (12) (2021) 1–11.
- [31] J. Gomez Socola, F.S. Rodrigues, Scintpi 2.0 and 3.0: low-cost GNSS-based monitors of ionospheric scintillation and total electron content, *Earth Planets Space* 74 (1) (2022) 185.
- [32] M. Bevis, S. Businger, T.A. Herring, R.A. Anthes, R.H. Ware, GPS meteorology: Remote sensing of atmospheric water vapor using the global positioning system, *Geophys. Mag.* 34 (1992) 359–425.
- [33] F. Ahmed, P. Vlacovic, F.N. Teferle, J. Douša, R. Bingley, D. Laurichesse, Comparative analysis of real-time precise point positioning zenith total delay estimates, *GPS Solut.* 20 (2) (2016) 187–199.

- [34] X. Li, G. Dick, C. Lu, M. Ge, T. Nilsson, T. Ning, J. Wickert, H. Schuh, Multi-GNSS meteorology: real-time retrieving of atmospheric water vapor from BeiDou, galileo, GLONASS, and GPS observations, *IEEE Trans. Geosci. Remote Sens.* 53 (12) (2015) 6385–6393.
- [35] S. Barindelli, E. Realini, G. Venuti, A. Fermi, A. Gatti, Detection of water vapor time variations associated with heavy rain in northern Italy by geodetic and low-cost GNSS receivers, *Earth Planets Space* 70 (1) (2018) 1–18.
- [36] A. Kriemeyer, M.-c. Ten Veldhuis, H. Marel, E. Realini, N. van de Giesen, Potential of cost-efficient single frequency GNSS receivers for water vapor monitoring, *Remote Sens.* 10 (2018) 1493, <http://dx.doi.org/10.3390/rs10091493>.
- [37] K. Stępnik, J. Paziewski, On the quality of tropospheric estimates from low-cost GNSS receiver data processing, *Measurement* 198 (2022) 111350, <http://dx.doi.org/10.1016/j.measurement.2022.111350>.
- [38] G. Marut, T. Hadas, J. Kaplon, E. Trzcina, W. Rohm, Monitoring the water vapor content at high spatio-temporal resolution using a network of low-cost multi-GNSS receivers, *IEEE Trans. Geosci. Remote Sens.* 60 (2022) 1–14, <http://dx.doi.org/10.1109/TGRS.2022.3226631>.
- [39] K. Larson, E. Small, E. Gutmann, A. Bilich, P. Axelrad, J. Braun, Using GPS multipath to measure soil moisture fluctuations: Initial results, *GPS Solut.* 12 (2008) 173–177, <http://dx.doi.org/10.1007/s10291-007-0076-6>.
- [40] K. Larson, E. Small, E. Gutmann, A. Bilich, J. Braun, V. Zavorotny, C. Larson, Use of GPS receivers as a soil moisture network for water cycle studies, *Geophys. Res. Lett.* 35 (2008) <http://dx.doi.org/10.1029/2008GL036013>.
- [41] K.M. Larson, E.D. Gutmann, V.U. Zavorotny, J.J. Braun, M.W. Williams, F.G. Nievinski, Can we measure snow depth with GPS receivers? *Geophys. Res. Lett.* 36 (17) (2009) <http://dx.doi.org/10.1029/2009GL039430>.
- [42] E.D. Gutmann, K.M. Larson, M.W. Williams, F.G. Nievinski, V. Zavorotny, Snow measurement by GPS interferometric reflectometry: an evaluation at niwot ridge, colorado, *Hydrol. Process.* 26 (19) (2012) 2951–2961, <http://dx.doi.org/10.1002/hyp.8329>.
- [43] J.L. McCreight, E.E. Small, K.M. Larson, Snow depth, density, and SWE estimates derived from GPS reflection data: Validation in the western U. S., *Water Resour. Res.* 50 (8) (2014) 6892–6909, <http://dx.doi.org/10.1002/2014WR015561>.
- [44] C.C. Chew, E.E. Small, K.M. Larson, V.U. Zavorotny, Effects of near-surface soil moisture on GPS SNR data: Development of a retrieval algorithm for soil moisture, *IEEE Trans. Geosci. Remote Sens.* 52 (1) (2013) 537–543.
- [45] S. Vey, A. Güntner, J. Wickert, T. Blume, M. Ramatschi, Long-term soil moisture dynamics derived from GNSS interferometric reflectometry: a case study for sutherland, South Africa, *GPS Solut.* 20 (4) (2016) 641–654.
- [46] C. Chew, E.E. Small, K.M. Larson, An algorithm for soil moisture estimation using GPS-interferometric reflectometry for bare and vegetated soil, *GPS Solut.* 20 (3) (2016) 525–537.
- [47] M.A.R. Fagundes, I. Mendonça-Tinti, A.L. Ieschek, D.M. Akos, F. Geremia-Nievinski, An open-source low-cost sensor for SNR-based GNSS reflectometry: Design and long-term validation towards sea-level altimetry, *GPS Solut.* 25 (2) (2021) 1–11.
- [48] Y. Li, K. Yu, T. Jin, X. Chang, Q. Wang, J. Li, Development of a GNSS-IR instrument based on low-cost positioning chips and its performance evaluation for estimating the reflector height, *GPS Solut.* 25 (4) (2021) 1–12.
- [49] M.A. Karegar, J. Kusche, F. Geremia-Nievinski, K.M. Larson, Raspberry pi reflector (RPR): A low-cost water-level monitoring system based on GNSS interferometric reflectometry, *Water Resour. Res.* (2021) e2021WR031713.
- [50] Z. Liu, L. Du, P. Zhou, Z. Liu, Z. Zhang, Z. Xu, Performance assessment of GNSS-IR altimetry using signal-to-noise ratio data from a huawei P30 smartphone, *GPS Solut.* 26 (2) (2022) 1–10.
- [51] K. Ichikawa, T. Ebinuma, M. Konda, K. Yufu, Low-cost GNSS-r altimetry on a UAV for water-level measurements at arbitrary times and locations, *Sensors* 19 (5) (2019) <http://dx.doi.org/10.3390/s19050998>.
- [52] R. Imam, M. Pini, G. Marucco, F. Dominici, F. Dovis, UAV-based GNSS-R for water detection as a support to flood monitoring operations: A feasibility study, *Appl. Sci.* 10 (1) (2020) <http://dx.doi.org/10.3390/app10010210>, URL <https://www.mdpi.com/2076-3417/10/1/210>.
- [53] T. Nilsson, J. Böhm, D. Wijaya, A. Tresch, V. Nafisi, H. Schuh, Path delays in the neutral atmosphere, in: J. Böhm, H. Schuh (Eds.), *Atmospheric Effects in Space Geodesy*, Springer Atmospheric Sciences, Springer, Berlin, Heidelberg, 2013, pp. 73–136.
- [54] J. Saastamoinen, Contributions to the theory of atmospheric refraction., *Bull. Geod.* 105 (1972) 13–34.
- [55] J. Boehm, A. Niell, P. Tregoning, H. Schuh, Global mapping function (GMF): A new empirical mapping function based on numerical weather model data, *Schuh. Geophys. Res. Lett.* 25 (2006) <http://dx.doi.org/10.1029/2005GL025546>.
- [56] D. Landskron, J. Böhm, VMF3/GPT3: refined discrete and empirical troposphere mapping functions, *J. Geod.* 92 (4) (2018) 349–360, <http://dx.doi.org/10.1007/s00190-017-1066-2>.
- [57] M.F. Glaner, Towards instantaneous PPP convergence using multiple GNSS signals (Ph.D. thesis), Department für Geodäsie und Geoinformation / Höhere Geodäsie, TU Wien, 2022, <http://dx.doi.org/10.34726/hss.2022.73610>, URL <https://repositum.tuwien.at/handle/20.500.12708/95695>.
- [58] J. Böhm, S. Böhm, J. Boissits, A. Girdiuk, J. Gruber, A. Hellerschmied, H. Krásná, D. Landskron, M. Madzak, D. Mayer, J. McCallum, L. McCallum, M. Scharntner, K. Teke, Vienna VLBI and satellite software (VieVS) for geodesy and astrometry, *Publ. Astron. Soc. Pac.* 130 (986) (2018) 044503, <http://dx.doi.org/10.1088/1538-3873/aaa22b>, URL <https://iopscience.iop.org/article/10.1088/1538-3873/aaa22b>.
- [59] D. Landskron, J. Böhm, Refined discrete and empirical horizontal gradients in VLBI analysis, *J. Geod.* 92 (12) (2018) 1387–1399, <http://dx.doi.org/10.1007/s00190-018-1127-1>.
- [60] T. Hadas, T. Hobiger, P. Hordyniec, Considering different recent advancements in GNSS on real-time zenith troposphere estimates, *GPS Solut.* 24 (2020) <http://dx.doi.org/10.1007/s10291-020-01014-w>.
- [61] C. Klasa, M. Arpagaus, A. Walser, H. Wernli, An evaluation of the convection-permitting ensemble COSMO-E for three contrasting precipitation events in Switzerland, *Q. J. R. Meteorol. Soc.* 144 (712) (2018) 744–764, <http://dx.doi.org/10.1002/qj.3245>.
- [62] K. Wilgan, A. Geiger, High-resolution models of tropospheric delays and refractivity based on GNSS and numerical weather prediction data for alpine regions in Switzerland, *J. Geod.* (2018) <http://dx.doi.org/10.1007/s00190-018-1203-6>.
- [63] G. Matheron, *Traité de Géostatistique Appliquée*. 2. Le Krigeage, Editions Technip, 1963.
- [64] B.S. Murphy, PyKrig: Development of a Kriging toolkit for Python, in: *AGU Fall Meeting Abstracts*, Vol. 2014, 2014, pp. H51K–0753.
- [65] N. Cressie, The origins of kriging, *Math. Geol.* 22 (1990) 239–252.
- [66] C. Roesler, K. Larson, Software tools for GNSS interferometric reflectometry (GNSS-IR), *GPS Solut.* 22 (2018) <http://dx.doi.org/10.1007/s10291-018-0744-8>.
- [67] K.M. Larson, J.J. Braun, E.E. Small, V.U. Zavorotny, E.D. Gutmann, A.L. Bilich, GPS multipath and its relation to near-surface soil moisture content, *IEEE J. Sel. Top. Appl. Earth Obs. Remote Sens.* 3 (1) (2009) 91–99.
- [68] H. Mittelbach, S.I. Seneviratne, A new perspective on the spatio-temporal variability of soil moisture: temporal dynamics versus time-invariant contributions, *Hydrol. Earth Syst. Sci.* 16 (7) (2012) 2169–2179, <http://dx.doi.org/10.5194/hess-16-2169-2012>, URL <https://hess.copernicus.org/articles/16/2169/2012/>.
- [69] G. Guerova, J. Douša, T. Dimitrova, A. Stoycheva, P. Václavovic, N. Penov, GNSS storm nowcasting demonstrator for Bulgaria, *Remote Sens.* 14 (15) (2022) <http://dx.doi.org/10.3390/rs14153746>.
- [70] T. Ning, J. Wang, G. Elgered, G. Dick, J. Wickert, M. Bradke, M. Sommer, R. Querel, D. Smale, The uncertainty of the atmospheric integrated water vapour estimated from GNSS observations, *Atmos. Meas. Tech.* 9 (1) (2016) 79–92, <http://dx.doi.org/10.5194/amt-9-79-2016>, URL <https://amt.copernicus.org/articles/9/79/2016/>.
- [71] W.T. Crow, A.A. Berg, M.H. Cosh, A. Loew, B.P. Mohanty, R. Panciera, P. de Rosnay, D. Ryu, J.P. Walker, Upscaling sparse ground-based soil moisture observations for the validation of coarse-resolution satellite soil moisture products, *Rev. Geophys.* 50 (2) (2012) <http://dx.doi.org/10.1029/2011RG000372>.